

WILEY-VCH

Multifunctional optoelectronic synapse based on ferroelectric van der Waals heterostructure
for emulating the entire human visual system

Feng Guo, Menglin Song, Man-Chung Wong, Ran Ding, Weng Fu Io, Sin-Yi Pang, Wenjing Jie and Jianhua Hao**

F. Guo, M. Song, M. Wong, R. Ding, W. Io, S. Pang, Prof. J. Hao

Department of Applied Physics, The Hong Kong Polytechnic University, Hung Hom,
Kowloon, Hong Kong 999077, P. R. China

E-mail addresses: jh.hao@polyu.edu.hk

W. Jie

College of Chemistry and Materials Science, Sichuan Normal University, Chengdu 610066,
P. R. China

E-mail addresses: wenjing.jie@sicnu.edu.cn

Keywords: ferroelectric two-dimensional material, van der Waals heterostructure, artificial
visual system, optoelectronic synapse, logic function, memory

This is the peer reviewed version of the following article: Guo, F., Song, M., Wong, M.-C., Ding, R., Io, W. F., Pang, S.-Y., Jie, W., Hao, J., Multifunctional Optoelectronic Synapse Based on Ferroelectric Van der Waals Heterostructure for Emulating the Entire Human Visual System. *Adv. Funct. Mater.* 2022, 32, 2108014, which has been published in final form at <https://doi.org/10.1002/adfm.202108014>. This article may be used for non-commercial purposes in accordance with Wiley Terms and Conditions for Use of Self-Archived Versions. This article may not be enhanced, enriched or otherwise transformed into a derivative work, without express permission from Wiley or by statutory rights under applicable legislation. Copyright notices must not be removed, obscured or modified. The article must be linked to Wiley's version of record on Wiley Online Library and any embedding, framing or otherwise making available the article or pages thereof by third parties from platforms, services and websites other than Wiley Online Library must be prohibited.

Abstract

The development of optoelectronic synapses could provide an important breakthrough toward creating a sophisticated and adaptable artificial visual system analogous to that of humans. However, it still remains a great challenge to implement the various functions of the biological visual neuromorphic system at the single device level. Intriguingly, two-dimensional (2D) van der Waals (vdW) heterostructure may offer a platform to address the issue. Here, a novel multifunctional synaptic device based on ferroelectric α -In₂Se₃/GaSe vdW heterojunction is proposed to emulate the entire biological visual system. Essential synaptic behaviors were observed in response to light and electrical stimuli; additionally, the retina-like selectivity for light wavelengths and the achievement of Pavlov's dog experiment demonstrate the device's capacity for processing complex electrical and optical inputs. Beyond the optoelectronic synaptic behaviors, the device incorporates memory and logic functions analogous to those in brain's visual cortex. The results of artificial neural network simulations show that the vdW heterojunction-based device is completely capable of performing logic operations and recognizing image with a high degree of accuracy. The work indicates that our versatile devices with a rational designed construction have great potential for efficiently processing complex visual information and may simplify the design of artificial visual systems.

1. Introduction

Artificial visual system, as a sub-discipline of artificial intelligence, has been applied to image recognition, autonomous vehicle driving, robotics, which not only convert light signals to internal information, but also needs to process and respond quickly to sensor inputs.^[1-4] In general, charge-coupled device (CCD) cameras or complementary metal-oxide silicon (CMOS) imagers as vision sensors are used to convert external light stimuli into electrical signals for image recognition based on neural network algorithms in computer.^[5] This means that current artificial visual systems' processors and memories are unable to respond directly to external light stimuli, and the conversion and transmission of signals in the vision sensor consume additional energy and induce signal latency. Therefore, there is a high demand for multi-functional artificial visual devices that can combine visual perception, data storage, and computation in a single device for handling a task of staggering complexity. In addition, due to the physically separated processing unit and memory in von Neumann computer, it is difficult for current artificial visual systems to implement real-time and accurate processing of continuous, high-throughput input signals generated by vision sensors with efficient energy utilization.^[6] In contrast, the flexible and sophisticated human visual system which consist of retina, optic nerve and visual cortex performs impressive feats. After visual signals processed in the retina, the stimuli are transmitted by the optic nerve to visual cortex where visual information can be processed in parallel and respond in real time with high efficiency and elegance. Artificial visual system that mimics humans, like other bionics success stories,^[7] provides a realistic solution for visual signal processing.

As a result, considerable effort has been devoted in developing artificial visual devices that mimic biological neural behaviors such as synaptic short-term plasticity (STP) and long-term plasticity (LTP).^[8, 9] Photonic synaptic behaviors including interpreting light signals and extract pertinent information, such as intensity and frequency, have been accomplished in an optoelectronic synapse based on photogating effect or persistent photoconductivity phenomenon.^[10-13] For example, fully photon modulated device based on ZnO/PbS heterostructure and solar-blind SnO₂ nanowire photo-synapse were proposed respectively to emulate plasticity functions of visual neuro.^[14,15] In addition to conventional semiconductor, two-dimensional (2D) layered materials have sparked great interest of researchers due to their superior optoelectronic properties since the discovery of graphene and transition metal dichalcogenides (TMDs).^[16-18] Because it is free from concerns about lattice mismatching in

van der Waals (vdW) heterojunctions, photogating effect is readily achieved in 2D materials-based optoelectronic synaptic devices. However, most proposed optoelectronic synaptic devices at the moment simply mimic the synapses that provide connections between neurons, and few previous works have attempted to functionalize them beyond their synaptic behaviors, for example, by integrating them with data storage and processing functions like those found in human visual cortex. Furthermore, the versatile optoelectronic synaptic device with a simple structure can be a powerful solution for future emulation of more complex neural systems. Conventional oxide-based ferroelectric materials with spontaneous electric polarizations have extensively been used in memory and logic devices for decades. Unique ferroelectricity provides an additional degree of freedom to functionalize devices, and synapses consisting of conventional ferroelectrics and 2D materials have also been investigated.^[12, 19] Nevertheless, the low conductivity and wide energy band gap of oxide ferroelectrics limit their application in optoelectronic synapses. Fortunately, the recent emergence of semiconducting vdW layered α - In_2Se_3 with narrow band gap of 1.4 eV exhibits robust ferroelectricity at room temperature even down to atomic scale, which offers the possibility to achieve efficient perception and processing of visual information for emulating the entire human visual system.

Here, optoelectronic synaptic (OES) device is proposed based on n-type ferroelectric α - In_2Se_3 and p-type 2D material GaSe heterojunction, which features biological behaviors of synapse, memory and logic functions. The detection of light stimuli and transmission of electrical stimuli are achieved by mimicking the retinal and electrical synapses, respectively. Besides, the success of known Pavlovian classical conditioning conducted to mimic associative learning in the human brain implies that the OES device is fully capable of handling multi-input signals. Furthermore, the realization of logic and memory functions enables optical sensing and neuromorphic function of visual cortex within a single device for multi-functionalization.

2. Results and Discussion

A biological synapse is the most fundamental link in a neural network, transmitting excitatory signals via chemical neurotransmitters from the presynaptic terminal to the postsynaptic terminal.^[20] The timing and strength of spikes can determine the tightness of connection, known as the weight of synapses. In the visual system of humans, synapses transmit electrical signals, which are generated by the retina under light stimuli, to the visual cortex of the brain for information storage and signal processing (**Figure 1a**).^[21] In this study, a vdW-hybrid synaptic three-terminal device was created to successfully emulate the entire biological

visual system's response to external light stimuli as well as the processing of input signals with excellent synaptic features. The structure of the OES device is depicted in Figure 1b, where three Au electrodes were first prepared on a Si/SiO₂ substrate, the source and drain were defined as presynaptic and postsynaptic terminals, respectively, while another one was used as a top gate. Before GaSe connected the channel and top gate, α -In₂Se₃ was deposited on the source and drain electrodes as a channel by dry transfer for transmitting synaptic excitation. Due to the intrinsic spontaneous polarization, ferroelectric materials have been widely used as memory devices, pressure sensors and photovoltaic solar cells.^[22-24] However, it is difficult to maintain Moore's law with the miniaturization of devices for conventional oxide dominant ferroelectric materials because of the critical thickness problem.^[25] The emergence of 2D vdW ferroelectric materials provides a solution to the problem. Unlike other 2D ferroelectric materials, which only involve pure in-plane (IP) or out of plane (OOP) orientations, semiconducting α -In₂Se₃ exhibits reversible spontaneous electric polarization in both IP and OOP orientations under room temperature.^[26-29] The strong interrelated coupling between the IP and OOP polarizations originates from the central Se atomic layer's lateral movement caused by an external electric field. Besides, the ferroelectric α -In₂Se₃ has two different stacking modes named rhombohedral (3R) and hexagonal (2H),^[30] which belong to the space group of R3m and P63/mmc, respectively, as shown in Figure 1c. Based on the high-resolution top-view, side-view TEM (Figure 1d, Figure S1) and the crystal structure model, it can be deduced that the α -In₂Se₃ used in this study has 3R stacking mode. In order to investigate the ferroelectricity of α -In₂Se₃, a nanosheet exfoliated from the bulk was transferred to a conductive Pt substrate, and piezoresponse force microscopy (PFM) was used to measure the amplitude and phase which were determined by magnitude of the local piezoelectric response and ferroelectric domain's polarization orientation, respectively. Figure 1e depicts the topographic, phase, and amplitude images obtained in Dual AC Resonance-Tracking (DART) mode of PFM, revealing a distinct phase and amplitude contrast in the area denoted by the arrow. The variation of amplitude and phase where the arrows are located can be clearly observed in Figure 1f. Moreover, the piezoelectric and amplitude loops are typical behaviors in ferroelectric materials, which reveal the dynamic process of ferroelectric domain reversal. The sharp change in parallelogram-like piezoelectric response loops and butterfly-like amplitude loop indicates the polarity is forced up or down under writing voltage (Figure 1g). In short, based on the above PFM measurement results and crystal structure analysis, it can be concluded that the α -In₂Se₃ nanosheets used in this study are intrinsically ferroelectric. Photoluminescence (PL) spectra were performed under

532 nm laser to measure the light absorption capacity of α -In₂Se₃ and GaSe. The laser intensity was limited to 1 mW in order to avoid damaging the 2D materials. According to Figure. 1h, i, the PL peak of α -In₂Se₃ is located at 870 nm and that of GaSe is 620 nm, indicating that hybrid structure device can absorb both visible and near-infrared light.

Figure 2a, b depicts the structure of an optic nerve as well as a side-view schematic diagram of the OES device. When the presynaptic neuron is excited, neurotransmitters will be released to the postsynaptic neuron, and the concentration of neurotransmitters determines whether the postsynaptic neuron ultimately generates postsynaptic current (PSC) or not. The weight of a synapse indicates the tightness of the connections between neurons, and it can be changed in response to neural activity called synaptic plasticity. Here, the channel conductance between the source and drain electrodes is defined as the synaptic weight which can be modulated by electrical and light inputs. The behaviors of electrical synapse are demonstrated in following part of Figure 2. As a type of short-term synaptic plasticity, paired-pulse facilitation (PPF) represents the influence of two consecutive spikes on synaptic weights. The inset of Figure 2c depicts the device being triggered by two consecutive electrical pulses (2 V, width 90 ms, interval 270 ms) and the PSC excited by the second electrical pulse is significantly higher, indicating strong facilitation. PPF can be quantified by the ratio of two PSCs, that is, $PPF\ index = [(A_2 - A_1)/A_1] \times 100\%$. As shown in the Figure 2c, the PPF index can reach up to 41% under minimum interval time, and index decreases exponentially as interval time increases. The behavior is similar to the enhancement of neurotransmitter release in a synapse.

The switch of ferroelectric polarization (P_{FE}) can be used to modulate the material's electrical properties. Thus, the conductance of OES devices based on ferroelectric semiconductors as channel can be tuned by switching the domains of α -In₂Se₃ with electrical pulses amplitude, which allow for the simulation of synaptic dynamics such as long-term potentiation/depression (LTP/LTD). As shown in Figure 2d, the conductance of the device channel increases from 6.21 nS to 9.70 nS after 20 consecutive electrical pulses (1 V, width 175 ms), and 20 discrete conductance states can be observed during the LTP process. For LTD, when negative voltage pulses were applied, the orientations of some domains were reversed, resulting in a gradual decrease of the conductance. To quantitatively evaluate and analyze the performance of OES devices, nonlinearity (NL), cycle to cycle variation (cyc) and symmetry were extracted from the above LTP/LTD curves. The NL and cyc were obtained by fitting the curves of LTP/LTD based on the Equation (1)-(3),^[31] where G_{LTP} and G_{LTD} represent the

conductance of LTP and LTD curves, respectively. The number of applied pulses is P , and the maximum value is expressed as P_{max} . Besides, the minimum and maximum conductance values are G_{min} and G_{max} . A indicates the magnitude of the LTP/LTD curve's nonlinearity. In addition, the symmetry is defined as LTD NL/LTP NL, so the ideal symmetry is 1. Here, 20 consecutive 1 V and -3 V voltages applied as an example has been shown in the Figure 2d named as case1. Moreover, the 2 V , -4 V (case 2) and 3 V, -5 V (case 3) are depicted in Figure S3. The details can be found in the radar plot (Figure 2e), which shows that all NLs remain below 4, with a minimum value of 2.21, very close to the ideal value of 1. Furthermore, regardless of how the electrical pulse amplitude varies, cycs are always kept below 2% and the maximum symmetry value is less than 1.6, indicating that the device performance does not change dramatically with the applied voltage, which is beneficial for reducing noise interference caused by read and write voltages. Because more discrete conductance states mean greater accuracy for hardware-based neural networks, 100 electrical pulses were applied to the OES device, as shown in Figure 2f. The increased number of pulses has no significant effect on degrading the device's performance when compared to 20 consecutive pulses, and the corresponding parameters will be discussed and applied in the following section about the neuromorphic computing simulation.

$$G_{LTP} = B \left(1 - e^{\left(\frac{-P}{A}\right)} \right) + G_{min} \quad (1)$$

$$G_{LTD} = -B \left(1 - e^{\left(\frac{P-P_{max}}{A}\right)} \right) + G_{max} \quad (2)$$

$$B = (G_{max} - G_{min}) / \left(1 - e^{\frac{-P_{max}}{A}} \right) \quad (3)$$

The working mechanism of the retina is shown schematically in **Figure 3a**. Figure 3b depicts a photonic synapse that mimics the retina, and its response characteristics were investigated by applying light stimuli. When the OES device was exposed to a light pulse, an increase in conductance can be observed, just like the retina can convert visible light into neural excitation. Photogenerated carriers resulted in an increase of channel conductance, and when the light stimulus was removed, the conductance decayed over time due to the photogating effect caused by the α -In₂Se₃/GaSe heterojunction. As can be seen in Figure 3c,d, similar to the PPF in the electric mode, the PSC produced by the second optical stimulus was significantly larger than that of the first, and the PPF index decreased exponentially to a small value as the interval time between the two stimuli increased. It is noteworthy that the OES device under light pulses has a longer decay time compared to electrical pulses because of two different

mechanisms. The former is caused by the reversal of the ferroelectric domains, but the latter is due to the photogating effect. Figure 3e depicts the trend of the PSC of OES device over time under 5, 10, and 20 light pulses (808 nm wavelength, 5.7 mW cm^{-2} , 1 s). It can be seen that the PSC increases as the number of light pulses increases and the decay time is prolonged. This is consistent with the phenomenon that the image remains in the biological visual system for a period of time after the removal of light stimulus, known as persistence of vision, which is the basis for the invention of film. The biological retina not only converts light stimuli into electrical signals, but also recognizes different colors, i.e., wavelength selectivity. However, most artificial optoelectronic synapses available currently can only respond to the density, number, and duration of light pulses.^[14, 15, 18] In the case of conventional vision sensors, additional accessories are generally required to achieve color recognition.^[32, 33] Here, the functions of sensing and color recognition are combined in the OES device. To investigate the operating mechanism of OES devices, 450 nm, 808 nm and 980 nm light pulses with the same density of 5.7 mW cm^{-2} were applied. As shown in Figure 3i, when a 450 nm light pulse was imposed on the OES device, the photocurrent rapidly saturates and can reach up to 52 nA, which is much higher than the case of 808 nm (Figure 3j). Additionally, almost no photogenerated current can be observed in the case of 980 nm (Figure 3k). Based on the PL spectra in Figure 1h,i and the energy band diagram of the p-n junction (Figure 3f-h), it is possible to conclude that the different PSC trends are primarily due to the two materials' different absorption abilities for different wavelengths of light. Thus, the biological retina's perceptual capability with color recognition is successfully implemented in this OES device.

As shown in **Figure 4**, the famous Pavlov's dog experiment was successfully conducted in device to mimic the classical conditioned reflex, which is widely used by animals and humans to associate different stimuli together. According to the above experimental results, light pulses can more easily induce larger PSCs than electrical pulses. Light pulses were thus defined as food (unconditioned stimulus) to cause salivation (unconditioned response), whereas electrical pulses were used to mimic the bell (conditioned stimulus) for the dog to trigger a conditioned response. In this case, a PSC of 7 nA was used as a threshold to determine whether the device had learned to associate electrical stimulus with light stimulus. Before training, 20 electrical pulses were used to mimic bell ringing (3 V, width 175 ms), as shown in Figure 4a, the PSC was eventually kept below the threshold, indicating that it did not cause salivation. A PSC of 10 nA, on the other hand, indicated that salivation could be sustained for a long time in response to a light pulse (18.7 mW cm^{-2} , width 7 s, 450 nm wavelength), implying that the dog's response

to food was distinct and strong as an unconditioned response (Figure 4b). Following that, Figure 4c depicts the training process for the dog, ringing the bell while feeding established a connection between the food and the bell. After trained, 20 electrical pulses were immediately applied to the OES device and the PSC can reach up to 8.9 nA, which is above the threshold value, as shown in Figure 4d. Subsequently, the electrical pulses were repeatedly applied every 120 s. As can be seen in the figure, the PSC gradually decreases with increasing time, that is consistent with the forgetting process in biological nervous system. The photogating effect is primarily responsible for the success of mimicking the classical conditioned reflex, in which a large number of photogenerated carriers are separated under light by the built-in electric field of α -In₂Se₃/GaSe heterojunction, and the carriers require a period of time to recombine after the pulses removed.

Because of their reversible polarization orientation that can be tuned by an applied electric field, ferroelectric materials are promising candidates for memory. In addition to conventional oxide ferroelectric materials, the emergence of 2D vdW semiconducting ferroelectric materials allows for device miniaturization, which has sparked the interest of researchers. In this section, memory function of the OES device based on ferroelectric α -In₂Se₃ is investigated, and the mechanism behind is discussed and analyzed carefully. To study the switch of ferroelectric domain with the applied electric field, the *I-V* curves were measured by sweeping the voltage from -2 V to 2 V, -4 V to 4 V and -6 V to 6 V in dark respectively, as shown in **Figure 5a**. Typical hysteresis loops are observed under different sweep voltages, with the arrows indicating the direction of the sweep. As far as we know, for devices based on α -In₂Se₃ channel, there are two different kinds of directions of current variation in the hysteresis loop with the applied sweep voltage. One case is shown in Figure 5b, where the currents of stage 1 and 3 in hysteresis loop are smaller than those of stage 2 and 4. Such hysteresis loops can be seen in devices whose metal electrodes are prepared on α -In₂Se₃ by E-beam, so that the surface and sides of α -In₂Se₃ are in contact with the metal, and energetic particles during the electrode preparation process may damage the interface between the metal and α -In₂Se₃.^[34] According to the literature, IP ferroelectricity is thought to play a dominant role in this case.^[35] In contrast, in this study, α -In₂Se₃ was transferred after the electrodes were prepared in order to form vdW contacts. The currents in stages 2 and 3 of the hysteresis loops are higher than those in stages 1 and 4 (Figure S4 and Figure 5a). We speculate that the difference in current change direction is primarily determined by whether OOP ferroelectricity plays a role, in which the bound charges on the top and bottom surfaces can act as a gate. Gu et al. proposed a planar device based on α -In₂Se₃ with

one electrode on the bottom surface of the left side and the other on the top surface of the right side, so that both IP and OOP ferroelectricity are considered to have an influence on the device.^[36] A hysteresis loop similar to our results was obtained in their work, which further suggests that our speculation about the influence of OOP ferroelectricity on the I - V curve is reasonable. Diode-like rectification behavior is observed, and the forward and reverse directions can be switched when a large voltage is applied to the device. As shown in Figure 5c, after imposing a -20 V electrical pulse (width 5 s), the direction of ferroelectric polarization (P_{FE}) points to the left side, which promotes the flow of current at negative voltage bias. The 50 periodic photoresponses up to ~ 0.1 pA are displayed in Figure 5d under light pulses (18.7 mW cm⁻², 0.1 Hz, 450 nm wavelength) at zero bias. The self-power characteristic can be attributed to the ferroelectric photovoltaic effect. When a 20 V voltage was applied to the device, the ferroelectric polarization direction was flipped to the right side, and the diode's rectification was also switched (Figure 5e). Figure 5f shows a lower photoresponse current than that of Figure 5d, which may be due to some ferroelectric domains not being fully reversed. Thus, the information stored in the OES device as memory can be read by light pulses nondestructively.

In order to add the capacity to process information, except sensing external stimuli and storing data, logic functions are highly desirable to be integrated in synaptic devices. Here, the light and electrical pulses are defined as input signals and the PSC represents the output value, **Figure 6a** demonstrates how light and electrical pulses are used to execute AND logic. For the accuracy of the logic function, "0" and "1" are carefully defined. Light switching (9.1 μ W cm⁻², 450 nm) determines the "1" and "0" of the logic input, and for electrical signals, the 0.1 V bias is considered as the "0", while the 3 V electrical pulse is the "1". When a "1" of the light signal and a "1" of the electrical signal were simultaneously applied to the synaptic device, the "1" of PSC output above threshold (30 nA) can be observed. The relatively large difference between the "0" and "1" states of PSC currents provides a broad range for defining thresholds as well improving logic operation accuracy. Based on the ferroelectricity of α -In₂Se₃, another logic function is provided, where the top gate divides the channel into left and right parts. The I - V curve of the p-GaSe/n-In₂Se₃ heterojunction is displayed in Figure 6b. The rectification behavior originates from the built-in electric field in heterojunction, and the hysteresis loop can be attributed to the reverse of ferroelectric polarization, which is typical in ferroelectric heterojunctions.^[37,38] When the polarization orientations of the left half channel is the same as that of right half, a photoresponse (~ 0.1 pA) under light pulses (450 nm wavelength, 18.7 mW cm⁻², period 10 s, width 3 s) at zero bias can be obtained from Figure 6c. The polarity of the

ferroelectricity in the right half of channel is reversed after an electrical pulse (15 V, 5 s) is applied between the top gate and the drain, as shown in Figure 6d, and no increase in PSC is observed under the light pulse. The coincidence of electrical and light signals may provide more possibilities for expanding additional logic functions in the synaptic devices.

Crossbar composed of synaptic devices, such as the OES device in this study, is a promising candidate to solve the bottleneck problem of von Neumann-based computing systems. By avoiding data movement and with the ability to compute in parallel manner, crossbar can dramatically reduce signal latency and thus improve computing efficiency. Figure 6e depicts the basic principle of crossbar, in which each input terminal is defined as a neuron in the input layer (X_i), and each output terminal is considered as a neuron in the output layer (Y_j), in addition, W_{ij} is used to represent the weight of synaptic device, which serves to connect the neurons. When voltage is applied to a programmable synaptic device, the conductance changes with the external voltage, and the crossbar can be used to mimic a neural network due to the additive nature of the current ($Y_j = \sum_{i=1}^n W_{ij} \times X_i$). To confirm the feasibility of the crossbar consisting of OES devices, an artificial neural network (ANN), which combines the device parameters extracted from Figure 2f, was created based on a software algorithm to simulate the behaviors of the crossbar and evaluate its performance. Here, XOR is chosen to train ANN for solving logic problems due to its unique nonlinearity compared to other logics. The ANN consists of input layer, hidden layer and output layer as shown in Figure 6f. The program code was written in Python according to the back propagation algorithm and with the help of neural core provided by crosssim platform.^[39] The program generates an 8×3 array and a 3×4 array at random in the first step to represent the weights between the input and hidden layers, the hidden and output layers, respectively. Next, the input values are propagated through the ANN (sigmoid is used as the activation function) to obtain the output values. After the difference between the output value and the target output value is multiplied by the input value and the learning rate (0.2), it is added to the original weight array to complete the update. The above process is repeated until the convergence criterion is met or the output value of ANN reaches the set target. Here the accuracy rate is calculated according to the Equation (4):

$$\text{Accuracy rate} = \left[1 - \frac{\sum_{i=1}^n |Y_{oi} - Y_{Ti}|}{n} \right] \times 100\% \quad (n=4) \quad (4)$$

where Y_o is the output value and Y_T is the target value. As can be seen in Figure 6g, the accuracy of the crossbar consisting of OES devices for XOR logic can be sustained at 90% after 1000

trainings, which is comparable to that of ideal software conditions (96%). To further verify the reliability of the crossbar, a Gaussian write noise is applied in the weight update process, and the results show that the rate of convergence is slowed down, but the final accuracy can also be close to 90%. In fact, ANN can make correct judgments as long as the accuracy rate is higher than 50%. Therefore, the neural network based on our proposed synaptic device is capable enough to perform logical computations. In addition, a larger neural network was built based on our device to perform image recognition and a high accuracy was obtained as shown in Figure S5.

3. Conclusions

In summary, a novel multifunctional optoelectronic synaptic device based on ferroelectric α -In₂Se₃/GaSe vdW heterojunctions is proposed to mimic the entire human visual system at the single device level. In electric modulation mode, plasticity functions of biological synapses such as PPF, LTP and LTD are achieved by switching the ferroelectric domains. The photonic synapse with wavelength selectivity suggests that our OES device not only converts light stimuli into electrical signals, but also possesses the capacity to recognize colors like the retina. Besides, the success of Pavlov's dog experiment further validates our device's ability to couple light and electrical signals, which allows us to mimic assisted learning in the human brain. More importantly, in addition to synaptic behaviors, logic functions and memory are integrated in the device with the help of unique ferroelectricity, thus accomplishing the task of mimicking the visual cortex. A high accuracy rate for XOR logic and image recognition was achieved in a simulated ANN, which demonstrates the reliability of the crossbar composed of our devices. Our work achieves a valuable breakthrough in emulating the entire human visual system using ferroelectric vdW heterojunction, and the multifunctional synaptic device proposed in this study offers significant potential in processing complex visual information.

4. Experimental Section

Device Fabrication: Ti/Au (10 nm/50 nm) metal electrodes were prepared on Si/SiO₂ (300 nm) substrates using a standard lithography technique and E-beam. Mechanical exfoliation was used to produce α -In₂Se₃ and GaSe nanosheets from bulk counterparts purchased from the HQ Graphene company. To construct α -In₂Se₃/GaSe vdW heterojunctions, α -In₂Se₃ nanosheets were placed on source and drain electrodes, and then GaSe nanosheets were transferred to connect α -In₂Se₃ channels and gate electrodes, the fabrication processes were performed by a dry transfer system equipped with a microscope.

Characterizations: Raman and PL spectra of the material were obtained by WITTEC_Confocal Raman system with a 532 nm laser at room temperature, and the laser intensity was set to less than 1 mW in order to avoid causing damage. Ferroelectricity was confirmed by PFM images of α -In₂Se₃ on a conductive Pt substrate using Asylum MFP 3D Infinity. The transmission electron microscope (TEM) image from Jeol JEM-2100F were used to analyze the lattice structure of α -In₂Se₃. Electrical characteristics were measured by Keithley 4200 in quiet mode. A waveform generator (Keithley 3390) was applied to produce light pulses. The power density of LED and lasers were calibrated by a power meter (Sanwa).

Neural Network Simulations: The program code was written in Python and combined with the neuron cores provided by the crosssim platform. The program ran under Spyder, a free integrated development environment (IDE).

Supporting Information

Supporting Information is available from the Wiley Online Library or from the author.

Acknowledgements

This research was supported by the grants from Research Grants Council of Hong Kong (GRF No. PolyU 153033/17P) and PolyU Postdoctoral Fellowships Scheme (YW4N). W. J. thanks support from the National Natural Science Foundation of China (61974097), Sichuan Youth Science and Technology Foundation (2019JDJQ0052).

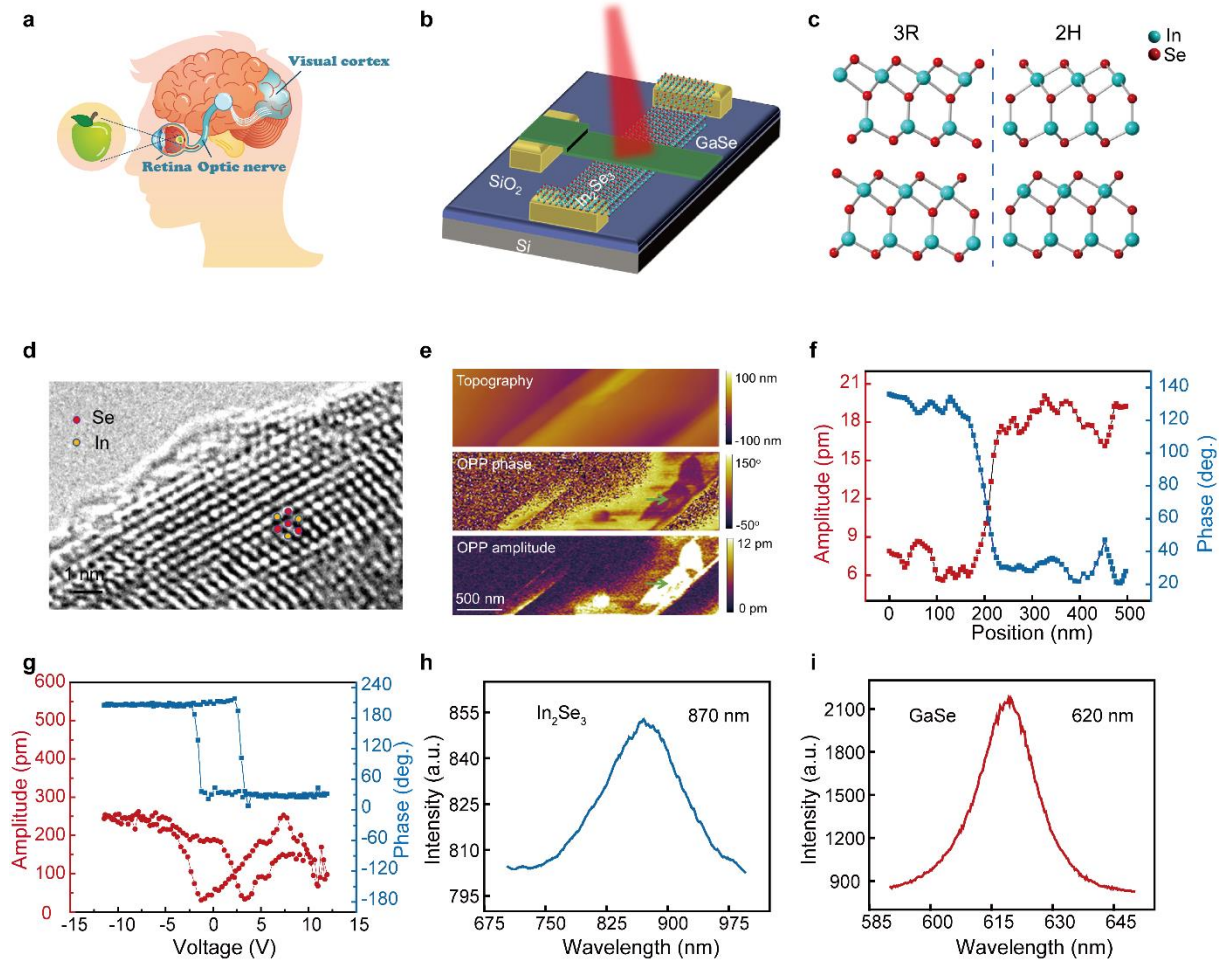


Figure 1. a) Schematic of entire biological visual system. b) The structure of proposed multifunctional optoelectronic synaptic device. c) Two different stacking modes of ferroelectric α - In_2Se_3 : rhombohedral (3R) structure and hexagonal (2H). d) TEM of a top-view α - In_2Se_3 nanosheet shows hexagonal symmetry. e) Topography, OOP PFM phase and OOP PFM amplitude images show opposite domain orientation (arrow location), scale bar is 500 nm. f) OOP PFM phase and OOP PFM amplitude along the arrow in e). g) PFM phase and PFM amplitude hysteresis loops of α - In_2Se_3 on Pt substrate indicate the switchable ferroelectric nature under external voltage. PL spectra of h) α - In_2Se_3 and i) GaSe under 532 nm laser.

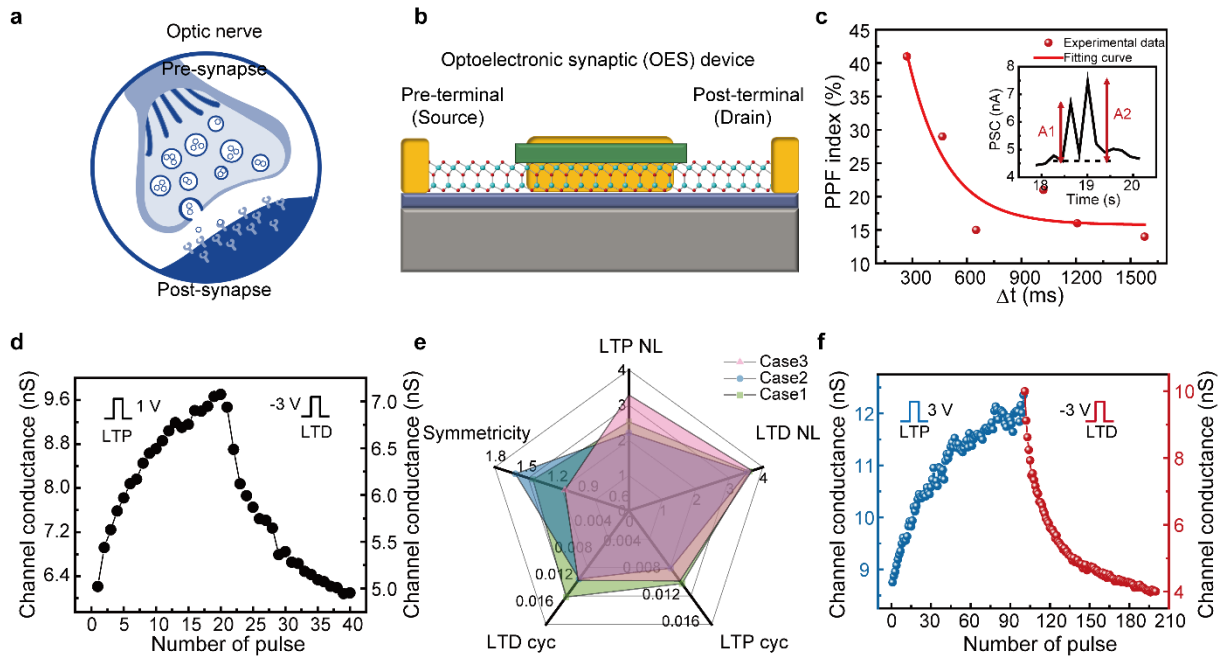


Figure 2. a) Schematic of optic nerve and b) A side-view diagram of the OES device. c) PPF index as a function of electrical pulse interval time Δt , the fitting curve shows that PPF decreases exponentially with the increase of Δt . The inset displays PSC triggered by two consecutive electrical pulses; A is defined as the amplitudes of PSC. d) LTP and LTD operations under 1 V (175 ms) as well as -3 V (175 ms) 20 applied pulses, respectively. e) Nonlinearity (NL), cycle to cycle variation (cyc) and symmetry of LTP and LTD under different cases: case1(1 V, -3 V), case2 (2 V, -4 V), case3 (3 V, -5 V). f) LTP and LTD operations under 3 V (175 ms) as well as -3 V (175 ms) 100 applied pulses, respectively.

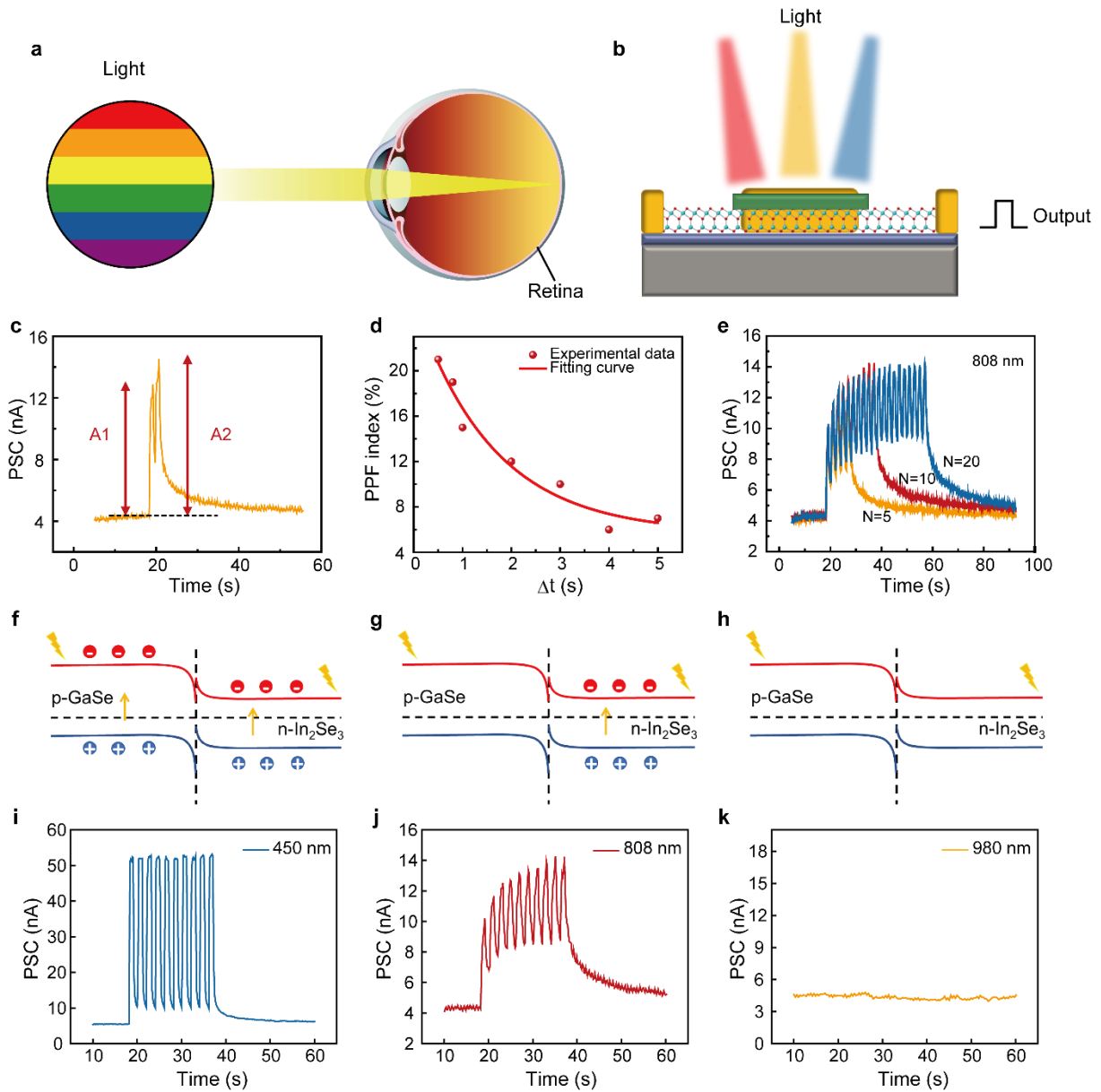


Figure 3. a) Working mechanism of the retina. b) Schematic of OES device under light pulses to mimics the retina. c) The PSCs triggered by a pair of light pulses (808 nm wavelength, 7.8 mW cm^{-2} , width 1 s) with $\Delta t=0.5$ s. d) PPF index as a function of light pulse interval time Δt . e) The PSC triggered by 5, 10 and 20 consecutive light pulses (808 nm wavelength, 5.7 mW cm^{-2} , 1 s). The different responses of PSC under 10 light pulses (5.7 mW cm^{-2} , 1 s) with i) 450 nm, j) 808 nm and k) 980 nm wavelength, respectively and related diagram of band structure f-h).

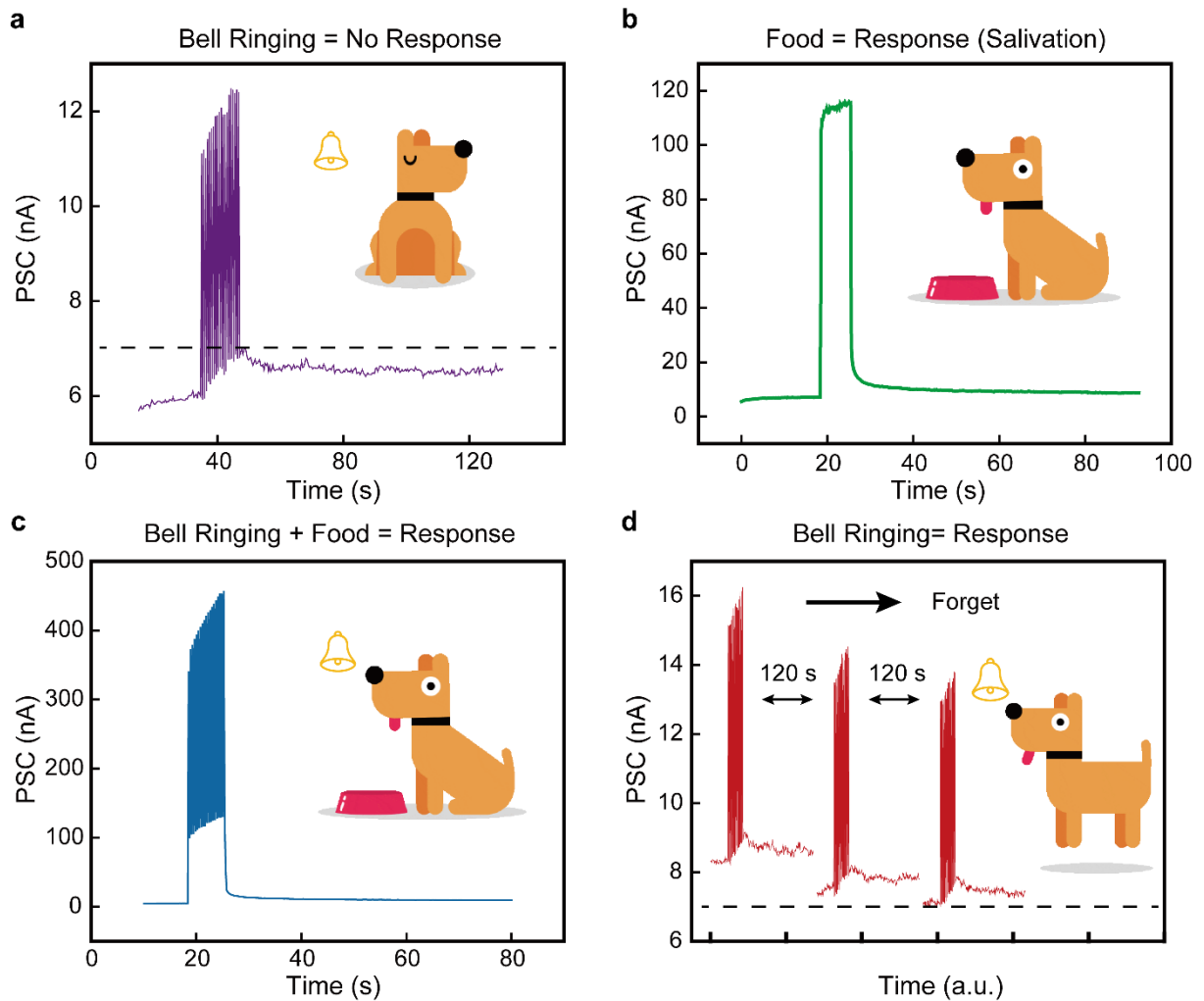


Figure 4. Pavlov's dog experiments to associate electrical and light stimuli together. a) 20 electrical pulses were applied, the PSC was below threshold of 7 nA (no response). b) A PSC of 10 nA was in response to a light pulse (18.7 mW cm^{-2} , width 7 s, 450 nm wavelength) (salivation). c) In order to couple different stimuli, the coincidence stimuli consist of electrical and light pulses were imposed on device. d) After training, electrical pulses alone can induce above-threshold PSCs. A forgetting behavior was observed with increasing time.

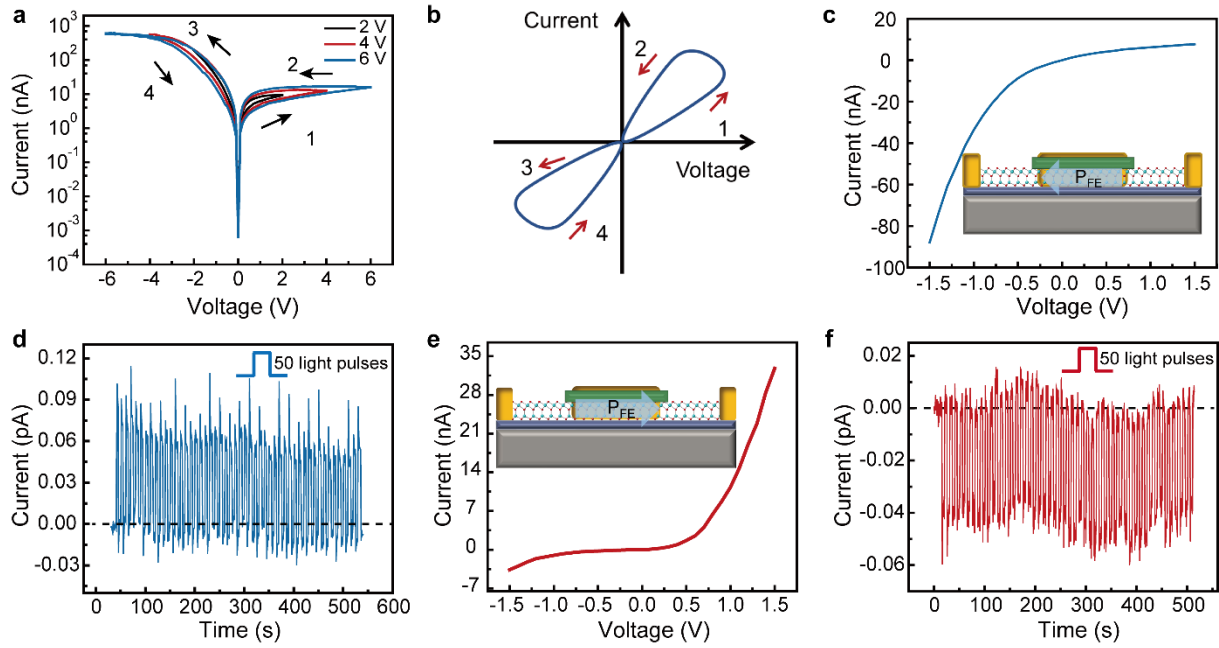


Figure 5. Memory function of OES device and read by light pulses. a) I - V hysteresis curves under sweep from 2 V to 6 V. b) The I - V curve where the currents of stage 1 and 3 in hysteresis loop are smaller than those of stage 2 and 4. c) I - V curve under ferroelectric polarization orientation shown in inset. d) Photoresponse at zero bias voltage under 50 light pulses (18.7 mW cm^{-2} , 0.1 Hz, 450 nm wavelength) and the ferroelectric polarization orientation in c). e) The I - V curve after a positive voltage applied, and f) corresponding photoresponse.

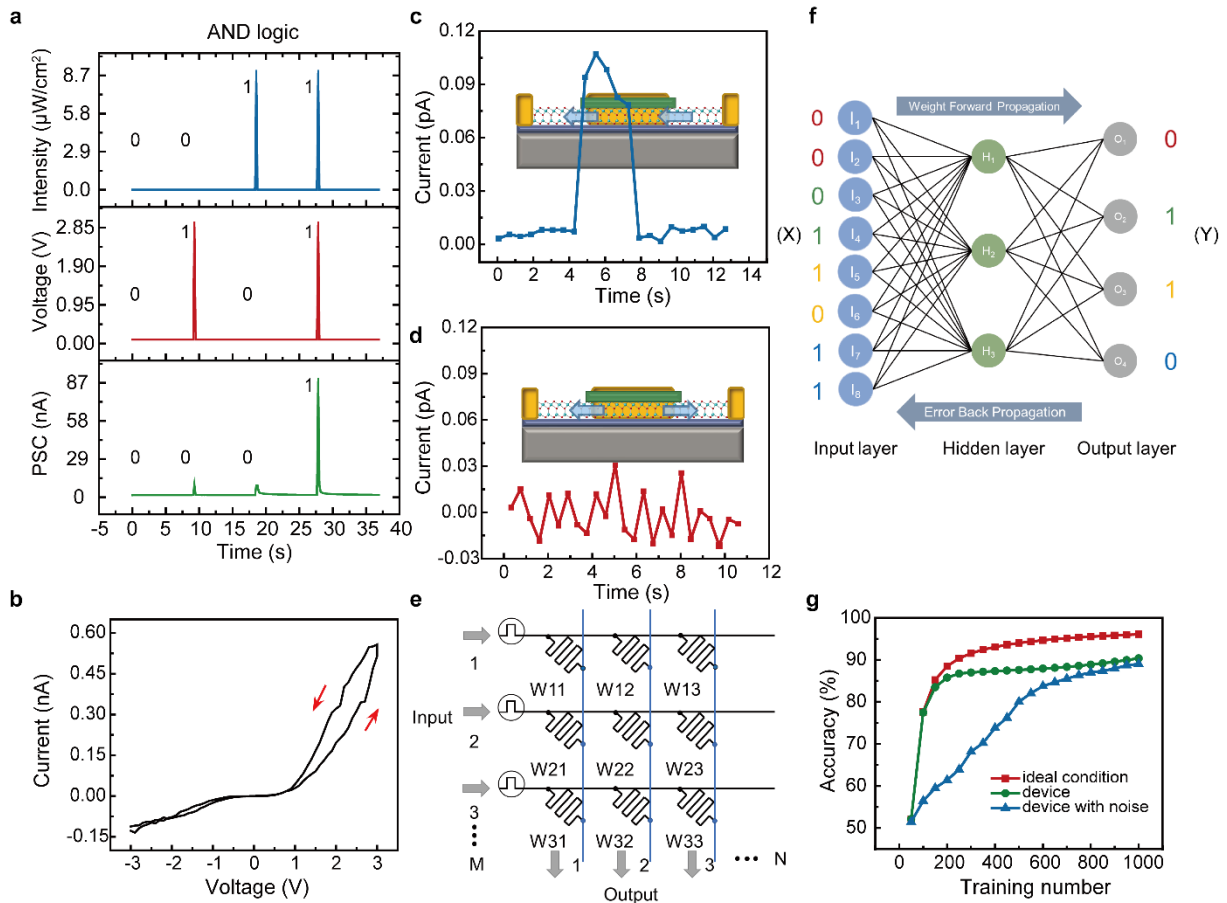


Figure 6. a) The “AND” logic function of device under light and electrical pulses. b) The I - V hysteresis curves of ferroelectric α - $\text{In}_2\text{Se}_3/\text{GaSe}$ vdW heterojunction. Photoresponse at zero bias voltage when the polarization orientations of two parts of channels are c) the same or d) opposite. The orientation of polarization is indicated by the arrows. e) The basic principle of crossbar. f) An ANN built to perform XOR logic. g) Accuracy rate as a function of training number.

Reference

- [1] L. Bodenhagen, A. R. Fugl, A. Jordt, M. Willatzen, K. A. Andersen, M. M. Olsen, R. Koch, H. G. Petersen, N. Kruger, *IEEE T. Autom. Sci. Eng.* **2014**, 11, 749.
- [2] G. A. M. Meiring, H. C. Myburgh, *Sensors-Basel* **2015**, 15, 30653.
- [3] S. Grigorescu, B. Trasnea, T. Cocias, G. Macesanu, *J. Field Robot* **2020**, 37, 362.
- [4] Y. Meng, F. Z. Li, C. Y. Lan, X. M. Bu, X. L. Kang, R. J. Wei, S. Yip, D. P. Li, F. Wang, T. Takahashi, T. Hosomi, K. Nagashima, T. Yanagida, J. C. Ho, *Sci. Adv.* **2020**, 6, 6389.
- [5] A. Kumar, *IEEE T. Ind. Electron.* **2008**, 55, 348.
- [6] Q. F. Xia, J. J. Yang, *Nat. Mater.* **2019**, 18, 309.
- [7] Y. Kim, A. Chortos, W. T. Xu, Y. X. Liu, J. Y. Oh, D. Son, J. Kang, A. M. Foudeh, C. X. Zhu, Y. Lee, S. M. Niu, J. Liu, R. Pfattner, Z. N. Bao, T. W. Lee, *Science* **2018**, 360, 998.
- [8] W. Huh, S. Jang, J. Y. Lee, D. Lee, D. Lee, J. M. Lee, H. G. Park, J. C. Kim, H. Y. Jeong, G. Wang, C. H. Lee, *Adv. Mater.* **2018**, 30, 1801447.
- [9] S. W. Luo, K. H. Liao, P. X. Lei, T. Jiang, S. Y. Chen, Q. Xie, W. B. Luo, W. Huang, S. G. Yuan, W. J. Jie, J. H. Hao, *Nanoscale* **2021**, 13, 6654.
- [10] F. C. Zhou, Z. Zhou, J. W. Chen, T. H. Choy, J. L. Wang, N. Zhang, Z. Y. Lin, S. M. Yu, J. F. Kang, H. S. P. Wong, Y. Chai, *Nat. Nanotechnol.* **2019**, 14, 776.
- [11] D. Y. Li, C. M. Li, N. Ilyas, X. D. Jiang, F. C. Liu, D. Gu, M. Xu, Y. D. Jiang, W. Li, *Adv. Intell. Syst.* **2020**, 2, 2000107.
- [12] Z. D. Luo, X. Xia, M. M. Yang, N. R. Wilson, A. Gruverman, M. Alexe, *Acs Nano* **2020**, 14, 746.
- [13] S. Seo, B. S. Kang, J. J. Lee, H. J. Ryu, S. Kim, H. Kim, S. Oh, J. Shim, K. Heo, S. Oh, J. H. Park, *Nat. Commun.* **2020**, 11, 3936
- [14] H. L. Li, X. T. Jiang, W. B. Ye, H. Zhang, L. Zhou, F. Zhang, D. H. She, Y. Zhou, S. T. Han, *Nano Energy* **2019**, 65, 104000.
- [15] Y. Chen, W. J. Qiu, X. W. Wang, W. R. Liu, J. X. Wang, G. Z. Dai, Y. B. Yuan, Y. L. Gao, J. Sun, *Nano Energy* **2019**, 62, 393.
- [16] A. K. Geim, *Science* **2009**, 324, 1530.
- [17] W. Choi, N. Choudhary, G. H. Han, J. Park, D. Akinwande, Y. H. Lee, *Mater. Today* **2017**, 20, 116.
- [18] S. Y. Wang, C. S. Chen, Z. H. Yu, Y. L. He, X. Y. Chen, Q. Wan, Y. Shi, D. W. Zhang, H. Zhou, X. R. Wang, P. Zhou, *Adv. Mater.* **2019**, 31, 1806227.
- [19] M. K. Kim, J. S. Lee, *Nano Lett.* **2019**, 19, 2044.

- [20] D. Choquet, A. Triller, *Neuron* **2013**, 80, 691.
- [21] S. Thorpe, D. Fize, C. Marlot, *Nature* **1996**, 381, 520.
- [22] R. Yang, *Nat. Electron.* **2020**, 3, 237.
- [23] Y. Lee, J. Park, S. Cho, Y. E. Shin, H. Lee, J. Kim, J. Myoung, S. Cho, S. Kang, C. Baig, H. Ko, *Acs Nano* **2018**, 12, 4045.
- [24] H. T. Huang, *Nat. Photonics* **2010**, 4, 134.
- [25] G. Gerra, A. K. Tagantsev, N. Setter, K. Parlinski, *Phys. Rev. Lett.* **2006**, 96, 107603.
- [26] W. J. Ding, J. B. Zhu, Z. Wang, Y. F. Gao, D. Xiao, Y. Gu, Z. Y. Zhang, W. G. Zhu, *Nat. Commun.* **2017**, 8, 14956.
- [27] Y. Zhou, D. Wu, Y. H. Zhu, Y. J. Cho, Q. He, X. Yang, K. Herrera, Z. D. Chu, Y. Han, M. C. Downer, H. L. Peng, K. J. Lai, *Nano Lett.* **2017**, 17, 5508.
- [28] F. Guo, Y. X. Lyu, M. B. Jędrzejczyk, Y. Q. Zhao, W. F. Io, G. X. Bai, W. Z. Wu, J. H. Hao, *Appl. Phys. Lett.* **2020**, 116, 113101.
- [29] W. F. Io, S. G. Yuan, S. Y. Pang, L. W. Wong, J. Zhao, J. H. Hao, *Nano Res.* **2020**, 13, 1897.
- [30] F. Xue, W. J. Hu, K. C. Lee, L. S. Lu, J. W. Zhang, H. L. Tang, A. Han, W. T. Hsu, S. B. Tu, W. H. Chang, C. H. Lien, J. H. He, Z. D. Zhang, L. J. Li, X. X. Zhang, *Adv. Funct. Mater.* **2018**, 28, 1803738.
- [31] P.-Y. Chen, X. Peng, S. Yu, IEEE International Electron Devices Meeting (IEDM) San Francisco, USA, Dec., **2017**.
- [32] K. H. Chung, Y. H. Chan, *IEEE T. Image Process.* **2008**, 17, 134.
- [33] W. Park, S. Pak, H. Shim, H. A. N. Le, M. Im, S. Chang, J. Yu, *Adv. Space Res.* **2016**, 57, 509.
- [34] Y. Liu, J. Guo, E. B. Zhu, L. Liao, S. J. Lee, M. N. Ding, I. Shakir, V. Gambin, Y. Huang, X. F. Duan, *Nature* **2018**, 557, 696.
- [35] B. Lv, Z. Yan, W. Xue, R. Yang, J. Li, W. Ci, R. Pang, P. Zhou, G. Liu, Z. Liu, W. Zhu, X. Xu, *Mater. Horiz.* **2021**, 8, 1472.
- [36] M. Gabel, Y. Gu, *Adv. Funct. Mater.* **2021**, 31, 2009999.
- [37] S. M. Poh, S. J. R. Tan, H. Wang, P. Song, I. H. Abidi, X. Zhao, J. D. Dan, J. S. Chen, Z. T. Luo, S. J. Pennycook, A. H. C. Neto, K. P. Loh, *Nano Lett.* **2018**, 18, 6340.
- [38] S. G. Yuan, Z. B. Yang, C. Xie, F. Yan, J. Y. Dai, S. P. Lau, H. L. W. Chan, J. H. Hao, *Adv. Mater.* **2016**, 28, 10048.
- [39] S. Agarwal, R. B. Jacobs-Gedrim, A. H. Hsia, D. R. Hughart, E. J. Fuller, A. A. Talin,

C. D. James, S. J. Plimpton, M. J. Marinella, IEEE Symposium on VLSI Technology Kyoto, Japan, June, **2017**.

ToC

To emulate entire human visual system at the single device level, a multifunctional optoelectronic synapse based on ferroelectric α -In₂Se₃/GaSe vdW heterostructure is elaborately designed. Visual perception, logic functions and memory are integrated in the device. Our work shed light on creating a sophisticated artificial visual system analogous to that of humans and break the bottleneck of current image recognition technology.

Feng Guo, Menglin Song, Man-Chung Wong, Ran Ding, Weng Fu Io, Sin-Yi Pang, Wenjing Jie* and Jianhua Hao*

Multifunctional optoelectronic synapse based on ferroelectric van der Waals heterostructure for emulating the entire human visual system

